PRODUCTION OF J/ψ IN MINIMUM-BIAS $p+p$ COLLISIONS AT $\sqrt{s} = 200$ GeV IN STAR*

Leszek Kosarzewski

for the STAR Collaboration

Faculty of Physics, Warsaw University of Technology
Koszykowa 75, 00-662 Warszawa, Poland

(Received December 15, 2011)

In this paper, the production of J/ψ in minimum-bias $p+p$ collisions at $\sqrt{s} = 200$ GeV in STAR is investigated. Low-p_{T} J/ψ in $p+p$ collisions can provide information about the production mechanism and serve as a reference for J/ψ production measurements in $A+A$ collisions. The invariant cross section is presented in the transverse momentum range of (0–3) GeV/c and the $\langle p_{\mathrm{T}}^2\rangle$ has been calculated. The J/ψ p_{T} spectrum is compared to Color Evaporation Model predictions and results from the PHENIX experiment at mid-rapidity. The results from STAR are consistent with Color Evaporation Model and PHENIX.

DOI:10.5506/APhysPolBSupp.5.543
PACS numbers: 13.20.Gd

1. Introduction

Suppression of J/ψ production was proposed as a signature of quark-gluon plasma formation in $A+A$ collisions [1]. The production of J/ψ in $p+p$ collisions can provide information about the production mechanism, which is still unknown, and can discriminate between theoretical models. It also serves as a baseline for measurements in heavy ion collisions, which are investigated by comparing the number of produced J/ψ per binary collision in $A+A$ with that in $p+p$.

Charm quarks are created primarily in the initial hard scattering phase of the collision. Charm quark production can be calculated with perturbative Quantum Chromodynamics (pQCD) methods. At a collision energy of $\sqrt{s} = 200$ GeV, the dominant process of charm production is via gluon

* Presented at the Conference "Strangeness in Quark Matter 2011", Kraków, Poland, September 18–24, 2011.

fusion. However, the formation of the bound state is a non-perturbative process. Various models have attempted to describe charm quark production and their hadronization into the J/ψ bound state. Such models include the Color Evaporation Model (CEM) [2], Color Singlet Model (CSM) [3] and Color Octet Model (COM) [4].

2. Data analysis

The data used in this analysis were from $p+p$ collisions at $\sqrt{s} = 200$ GeV collected by STAR experiment during 2009 running. A total of 74 million minimum-bias events were analysed. J/ψ particles are reconstructed in STAR through their dielectron decay channel ($J/\psi \to e^+e^-$) using the Time Projection Chamber (TPC) for tracking and particle identification. Other detectors used in this analysis are the Barrel Electromagnetic Calorimeter (BEMC) and the Time-of-Flight (TOF), which was 72% installed. Electrons are identified using their ionization energy loss (dE/dx) in the TPC. Figure 1 (left) shows the dE/dx distributions for all particles. The dE/dx has been normalized to the expected value for electrons $n\sigma_e$ using Eq. (1)

$$n\sigma_e = \log\left(\frac{dE/dx}{dE/dx_e\,|_{\rm Bichsel}}\right)\Big/\sigma\,. \tag{1}$$

The $dE/dx_e\,|_{\rm Bichsel}$ is the expected energy loss for an electron estimated using Bichsel [6] function, and σ is the TPC dE/dx resolution. Electrons are selected using $-1 < n\sigma_e < 2$. The asymmetric cut is used to reduce pion contamination with small $n\sigma_e$. TOF is used for hadron rejection up to particle momentum of 1.4 GeV/c. This allows us to obtain a very pure sample of electrons even in the regions where hadron and electron dE/dx overlap. The TOF is used to calculate particle $\beta = v/c$. For electrons

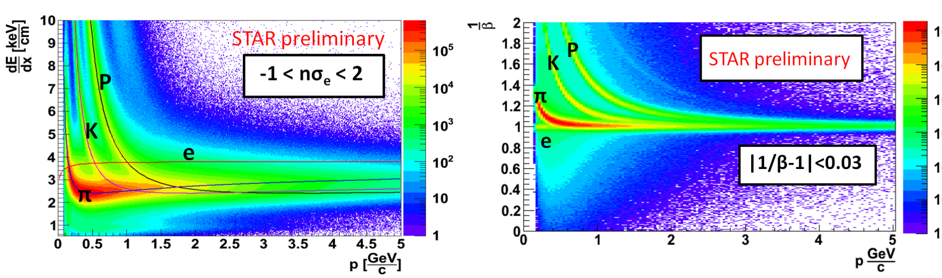

Fig. 1. Left: TPC dE/dx *vs.* momentum for all particles. Electrons are selected using $-1 < n\sigma_e < 2$. Right: TOF $1/\beta$ *vs.* momentum distributions for all particles. Kaons and protons are well separated from electrons up to ≈ 1.4 GeV/c. Electrons are identified using $|1/\beta - 1| < 0.03$.

$\beta \approx 1$. This allows the clear distinction of electrons from kaons and protons, using $|1/\beta - 1| < 0.03$ cut. The $1/\beta$ distribution from TOF is shown in Fig. 1 (right). The BEMC is used for electrons with $p > 2$ GeV/c. Electrons are expected to deposit all of their energy in electromagnetic calorimeter, so the $E/p \approx 1$, where E is the single tower ($\Delta\eta \times \Delta\phi = 0.05 \times 0.05$) energy. We require $E/p > 0.5$ to reject hadrons.

Electrons are combined into unlike-sign (e^+e^-) and like-sign (e^+e^+, e^-e^-) pairs and their invariant mass is calculated. This is shown in the left plot of Fig. 2. The unlike-sign pair invariant mass spectrum contains both signal and background. The background is estimated using the sum of like-sign pairs and subtracted from the unlike-sign pair distribution. The right plot in Fig. 2 shows the distribution after background subtraction. This distribution is fitted with a Gaussian function and a linear residual background to take the charm continuum into account. The number of reconstructed J/ψ is obtained from bin counting in the invariant mass range $3.0 < m_{e+e-} < 3.2$ GeV/c^2 after subtracting the residual background. The J/ψ are reconstructed in $|y| < 1$ and $p_{\rm T} < 3$ GeV/c. The uncorrected signal is 44 ± 8 J/ψ with a signal to background ratio of 2.8 and a significance of 5.7σ. To obtain the $p_{\rm T}$ spectrum, the yield is divided into 3 $p_{\rm T}$ bins: (0–1) GeV/c, (1–2) GeV/c, (2–3) GeV/c.

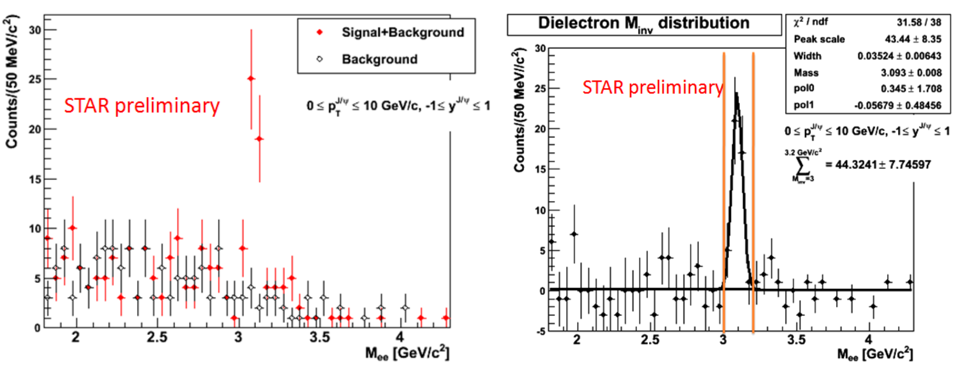

Fig. 2. The dielectron invariant mass distribution. The left plot shows the e^+e^- pairs (red full circles) and like sign combinatorial background made from e^+e^+ and e^-e^- pairs (black open circles). The right plot shows pair distribution after background subtraction. The fitted function is a Gaussian signal and a linear residual background.

In order to simulate the detector effects, simulated Monte Carlo electrons are embedded into real events and the whole STAR detector response is simulated. Each event is then reconstructed with the same algorithm that is used to reconstruct the real data. The single electron tracking efficiency and acceptance ($\epsilon_{\text{tracking}\times\text{acceptance}}$) is obtained by considering the fraction of electrons which are reconstructed after applying all analysis cuts. The single electron identification efficiency ϵ_{PID} includes E/p, $1/\beta$ and $n\sigma_e$ cut efficiencies obtained from the data. To calculate the σ_e cut efficiency, the $n\sigma_e$ distribution from the data is fitted with Gaussians for electrons, pions, kaons and protons. Then the fit parameters are used to reproduce the distributions from the data in a Monte Carlo simulation. The $-1 < n\sigma_e < 2$ cut is applied in the simulation to calculate the number of accepted electrons and the efficiency. The $E/p < 0.5$ cut efficiency is calculated from the data by selecting very pure electron sample from $\gamma \to e^+e^-$. The $|1/\beta - 1| < 0.03$ cut efficiency is obtained from the simulation. The total single electron correction is calculated with the Eq. (2)

$$\epsilon_e = \epsilon_{\text{tracking}\times\text{acceptance}} \times \epsilon_{\text{PID}} \,. \tag{2}$$

The total single electron efficiencies were applied to e^+ and e^- from J/ψ decays from PYTHIA to calculate the J/ψ reconstruction efficiency shown in Fig. 3. Final formula is presented as Eq. (3). All single electron corrections enter in quadrature to the J/ψ reconstruction efficiency. Also included is the trigger efficiency $\epsilon_{\text{trigger}}$ obtained from MC simulation

$$\epsilon_{J/\psi}\left(p_{\text{T}}^{J/\psi}\right) = \epsilon_{\text{trigger}} \times \epsilon_{e^+}\left(p_{\text{T}}^{e^+}\right) \times \epsilon_{e^-}\left(p_{\text{T}}^{e^-}\right) \,. \tag{3}$$

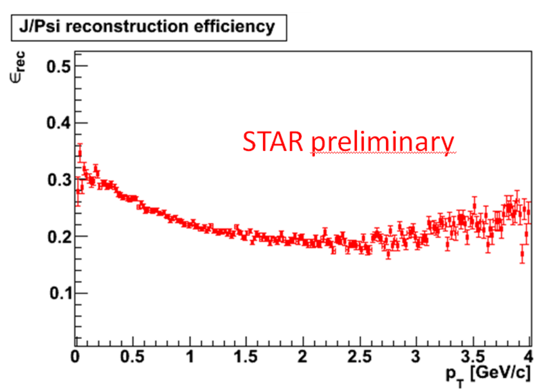

Fig. 3. The J/ψ reconstruction efficiency *vs.* p_{T}. It includes trigger efficiency, tracking efficiency, acceptance correction and electron identification efficiency.

The uncorrected signal is then corrected for the efficiency in each J/ψ p_{T} bin and the invariant cross section is calculated according to formula Eq. (4)

$$\frac{B_{ee}}{2\pi p_{\text{T}}}\frac{d\sigma^2_{J/\psi}}{dp_{\text{T}}dy} = \frac{1}{2\pi p_{\text{T}}}\frac{N^{\text{raw}}_{J/\psi}(p_{\text{T}})\sigma^{pp}_{\text{NSD}}}{\Delta y \Delta p_{\text{T}} N_{\text{events}}}\frac{1}{\epsilon_{J/\psi}(p_{\text{T}})} \,. \tag{4}$$

The $J/\psi \to e^+e^-$ branching ratio is $B_{ee} = 5.94 \pm 0.06\%$ [5], $N^{\rm raw}_{J/\psi}(p_{\rm T})$ is the raw number of J/ψ in each $p_{\rm T}$ bin, $\sigma^{pp}_{\rm NSD} = 30.0 \pm 3.5$ mb [7] is the $p+p$ non-single diffractive cross section and $\epsilon_{J/\psi}(p_{\rm T})$ is the total J/ψ reconstruction efficiency from the simulation.

3. Results

The J/ψ invariant cross section at low-$p_{\rm T}$ ($p_{\rm T} < 3$ GeV/c) is shown in Fig. 4 (black/blue stars). This is combined with STAR results [8] at higher $p_{\rm T}$ ($2 < p_{\rm T} < 8$ GeV/c). Both high-$p_{\rm T}$ and low-$p_{\rm T}$ results are used to obtain the integrated cross section. In the overlap range $2 < p_{\rm T} < 3$ GeV/c the high-$p_{\rm T}$ data are used because of higher statistics. The integrated cross section is $B_{ee}\frac{d\sigma_{J/\psi}}{dy}\big|_{|y|<1} = 40.6 \pm 6.0\,(\text{stat.})$ nb. After correction for bremsstrahlung tail of J/ψ (*i.e.* including J/ψ reconstructed with mass below 3 GeV), the final cross section is $B_{ee}\frac{d\sigma_{J/\psi}}{dy}\big|_{|y|<1} = 46.2 \pm 7.3\,(\text{stat.})$ nb.

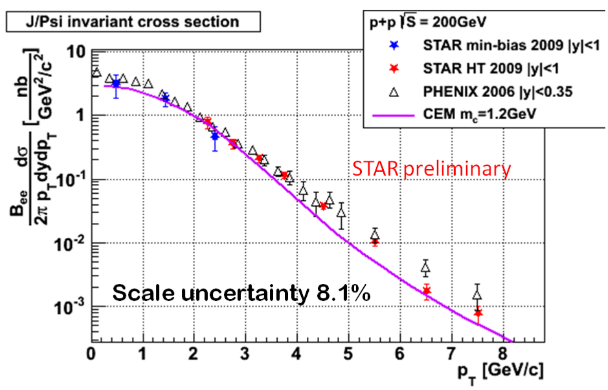

Fig. 4. The J/ψ $p_{\rm T}$ spectrum. Low-$p_{\rm T}$ (black/blue) and high-$p_{\rm T}$ (grey/red) [8] STAR results are compared to PHENIX data (triangles) [9] and CEM prediction (curve) [10].

The $\langle p_{\rm T}^2\rangle$ was extracted from the $p_{\rm T}$ spectrum using a power-law function described in Eq. (5). The $\langle p_{\rm T}^2\rangle$ is related to the energy density reached in a collision. The obtained value is listed in Eq. (6). Fig. 5 shows the $\langle p_{\rm T}^2\rangle$ as a function of $\sqrt{s}$. The STAR data is compared to other experiments [9]. The results are consistent with the PHENIX data at mid-rapidity

$$f(p_{\rm T}) = Ap_{\rm T}\left(1+(p_{\rm T}/B)^2\right)^{-6}, \quad (5)$$

$$\langle p_{\rm T}^2\rangle = 4.5 \pm 0.3\ {\rm GeV}^2/c^2\,. \quad (6)$$

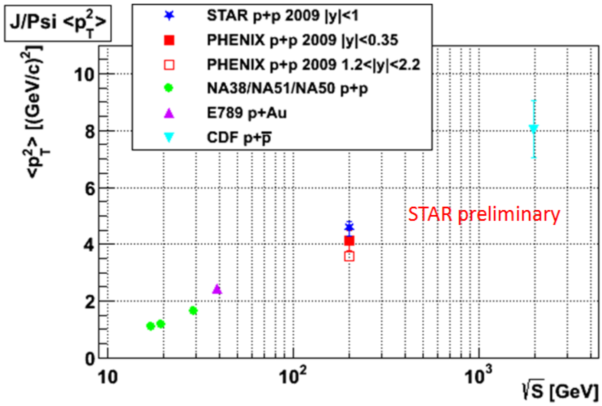

Fig. 5. J/ψ $\langle p_{\rm T}^2 \rangle$ as a function of $\sqrt{s}$ from different experiments [9].

4. Summary

The J/ψ production cross section, $p_{\rm T}$ spectrum and $\langle p_{\rm T}^2 \rangle$ measured by STAR at mid-rapidity were presented. The low-$p_{\rm T}$ spectrum was shown for $p_{\rm T} < 3$ GeV/c. Combined low-$p_{\rm T}$ and high-$p_{\rm T}$ results from STAR were used to calculate the integrated cross section. The low-$p_{\rm T}$ data are consistent with CEM model prediction. The results are also consistent with the results of the PHENIX experiment at mid-rapidity.

REFERENCES

[1] T. Matsui, H. Satz, *Phys. Lett.* **B178**, 416 (1986).
[2] J.F. Amundson *et al.*, *Phys. Lett.* **B390**, 323 (1997).
[3] J.P. Lansberg, *Phys. Lett.* **B695**, 149 (2011).
[4] P.L. Cho, A.K. Leibovich, *Phys. Rev.* **D53**, 6203 (1996).
[5] Particle Data Group, "Particle Physics Booklet", July 2010.
[6] H. Bichsel, Comparison of Bethe–Bloch and Bichsel Functions, STAR Note SN0439.
[7] J. Adams *et al.* [STAR Collaboration], *Phys. Lett.* **B612**, 181 (2005).
[8] Z. Tang [STAR Collaboration], `arXiv:1107.0532v1 [hep-ex]`.
[9] A. Adare *et al.*, *Phys. Rev. Lett.* **98**, 232301 (2007).
[10] A.D. Frawley, T. Ullrich, R. Vogt, *Phys. Rep.* **462**, 125 (2008); R. Vogt, private communication.